EASTERN SECTION
SEISMOLOGICAL
RESEARCH LETTERS

Finding Faults in the Charleston Area, South Carolina: 1. Seismological Data

Inmaculada Durá-Gómez and Pradeep Talwani
Department of Geological Sciences, University of South Carolina, Columbia

ABSTRACT

Macroscopic observations following the 1886 Charleston, South Carolina, earthquake and analyses of instrumentally recorded seismicity between 1974 and 2004 suggest the presence of two or more active faults. In order to more clearly define the active faults and determine their seismotectonic framework, instrumentally located hypocenters were relocated using the double-difference algorithm HypoDD. The revised hypocentral locations were associated with different faults based on the first motions recorded at different locations. The result is a plausible framework that shows several important changes from earlier interpretations. This framework defines a localized stressed volume, which consists of the ~50-km-long ~N30°E striking, NW dipping Woodstock fault associated with oblique right-lateral strike-slip motion with a ~6-km-long antidilatational left step near Middleton Place. Three ~NW-SE striking reverse faults, two NE dipping and one SW dipping, were recognized within this left step; of these, the NE dipping Sawmill Branch fault zone lying between Middleton Place and Summerville is the most active. Minor activity was observed on the NE dipping Lincolnville and the SW dipping Charleston faults. The southernmost Sawmill Branch fault zone also shows evidence of left-lateral strike-slip motion. The ~N55°W trending Ashley River fault lying between Middleton Place and the Magnolia Plantation appears to be currently inactive .

INTRODUCTION

The aim of this paper and its companion paper is to present a revised, plausible seismogenic framework to explain the 1886 Charleston, South Carolina, earthquake and ongoing seismic activity in the Charleston area. The exact nature of the causative faults was largely unknown because the earthquakes occur below subsurface Triassic-age basalt flows and there is a general absence of a surface expression of faults. However, in the past three decades a variety of multidisciplinary data have become available and have led to an improved understanding of surface and subsurface features that may be related to the seismicity. In this paper we present a plausible seismotectonic framework based on the analysis of seismicity data collected over three decades, complemented and constrained by geological, geophysical, geomorphological, and geodetic data. The details of these complementary data are presented in the companion paper.

The earliest information about seismic sources in the Charleston seismic zone came from the several descriptions of the macroscopic effects of the 1886 Charleston earthquake, which indicated that the seismicity was associated with multiple sources. These data are described in the next section. The next advance in our understanding occurred in the early 1970s with the deployment of a seismic network in the Charleston region. As the number and accuracy of hypocentral locations improved, so did our ideas of the causative faults. These improvements in the development of a seismogenic framework occurred in parallel with improvements in our understanding of the nature of intraplate earthquakes. These are described in the following sections and are the subject of this paper.

INFERENCES OF MULTIPLE SOURCES FROM THE REPORTS OF THE 1886 CHARLESTON EARTHQUAKE

The idea that multiple faults might be present in the Summerville area dates back to the studies carried out after the 1886 Charleston earthquake. Clarence E. Dutton, captain of the U.S. Ordnance Corps in charge of the earthquake investigation for the U.S. Geological Survey, Division of Volcanic

doi: 10.1785/gssrl.80.5.883

Geology, compiled a report that included first-hand accounts by C. McKinley, Dr. G. E. Manigault, and F. R. Fisher (Dutton 1890). Many of these accounts described a SW-NE direction of motion in Charleston, while chronicles in the Summerville area described mainly vertical motions. According to McKinley, associate editor of the *Charleston News and Courier*, on James Island, located a few miles south of Charleston, "the direction of the motion was reported to have been from the southwest, passing off towards the north" (Dutton 1890, 224). Manigault, curator of the College of Charleston, whose residence was located in the southwestern part of Charleston on the bank of the Ashley River, reported that his "impression as to the direction from which the waves came was that they reached me from a little south of west by the compass, and that they traveled to a little north of east" (Dutton 1890, 240–241). Vertical motion was extensively reported in Summerville. Manigault wrote that "these indications of what was coming were more distinct at the village of Summerville, about twenty miles from Charleston, on the line of the railroad to Augusta, Ga., and more distinct still at 'Ten Mile Hill,' on the same railroad; as both those places, especially the first, were afterwards the scenes of vertical thrusts" (Dutton 1890, 231). Other felt reports from Summerville compiled by Dutton stated that "the direction of its impulses was nearer the vertical than the horizontal… The injuries to chimneys were also very characteristic… in many cases, instead of being snapped off clean by a horizontal fracture, [chimneys] were broken along a highly inclined plane, as if sheared, and fell easily to the ground. There was a marked tendency to fall in a northwestern and southeastern direction, but instances could be found of chimneys falling in almost any direction" (Dutton 1890, 274). Among these felt reports, one written by Thomas Turner, president of the Charleston Gas Light Company, mentions that "the floor seemed to go down in front of me at an angle of twenty-five to thirty degrees. It was so sudden and unexpected, that I was thrown forward into the hall about 10 feet and as quickly thrown backwards" (Dutton 1890, 272).

More than one active fault in the area is also suggested by the entries in the diary of Ada Trotter, an Englishwoman familiar with earthquakes from her stay in Italy, who visited Summerville between 18 March 1887 and 2 May 1888 and kept a journal of the still-frequent aftershocks (Louderback 1943). There was continuing, audible seismicity that she associated with two different sources, one near and one distant. She usually described the earthquakes originating in the nearby source as loud explosions under the house. For example, on 24 March 1887 she wrote: "Was sitting in the Piazza when an explosive kind of rumbling sounded right under me. My chair shook slightly and I saw the Piazza was shaken too. Mr. Boyle came over and said he felt the earth move under his feet and that there was something very unusual in the character of the shake. Seems to me as though there was a dynamite factory in operation immediately under us and occasional explosions." Other entries in the diary relate to earthquakes coming from a more distant source. For example, on 28 March 1887 she wrote: "Near morning I think, but while it was quite dark, I was wakened by a loud rumbling and very slight shake. Scarcely five minutes later came a louder bang and quite a long shake though gentle. My bed shook back and forth, east and west. Things in the room rattled."

Adding to the story of Ada Trotter is the fact that she distinguished two different directions of shaking, which could be associated with two separate seismic sources. On 14 April 1887 she wrote: "Last night, (Wed. night) at 2:25 a rumbling and vigorous shake from north to south instead of as usual east to west. Was told this morning that a bomb! went off a little earlier, this is what probably awoke me, for I was awake when the one I record occurred."

First-hand accounts also brought up the possibility that the main shock was a "compound" shock. Manigault expressed to C. E. Dutton (Manigault, quoted in Dutton 1890) that "the impression produced upon many was that it could be subdivided into three distinct movements, while others were of the opinion that it was one continuous movement or succession of waves." Earle Sloan, a mining consultant at the time of the earthquake and who later was named assistant USGS geologist, explained the event as a compound shock with three epicenters, the first near the town of Woodstock, the second near Middleton Place (on the bank of the Ashley River), and the third west of Rantowles (see map in McKinley 1887, 442). Dutton reinterpreted the data gathered by Earle Sloan and concluded that the seismicity was associated with two seismic sources located near Woodstock and Rantowles (Figure 1).

MODERN ERA

During the twentieth century, various researchers have studied the causes of the 1886 Charleston earthquake. Their studies and conclusions are summarized in this section.

Taber (1914) suggested the 31 August 1886 earthquake was caused by differences in rainfall in the preceding months between Summerville and Charleston. The larger amount of rainfall near Summerville resulted in "readjustments taking place along a plane of faulting located in the crystalline basement underlying the Coastal Plain sediments, not far from Woodstock, and extending in a general northeast-southwest direction" (Figure 1).

Bollinger (1977) reassessed the 1886 earthquake intensity data to obtain two new isoseismal maps (on the Modified Mercalli Intensity scale) emphasizing the broad regional pattern of effects and the more localized variations of intensity, respectively. While previous intensity contours by Sloan, as cited in Dutton 1890, had not been labeled, Bollinger assigned intensity values to his contours and estimated that the maximum epicentral intensity was X on the Modified Mercalli Intensity scale. In addition, he estimated the body-wave magnitude to be 6.8 based on intensity-particle velocity data derived from central U.S. data or 7.1 based on western U.S. data. Assuming the value of 6.8 for the body-wave magnitude, he estimated the fault length, fault width, and average slip to be 25 km, 12 km, and 1 m respectively (Bollinger 1983). Current estimates of the magnitude of the 1886 earthquake, based on isoseismal data,

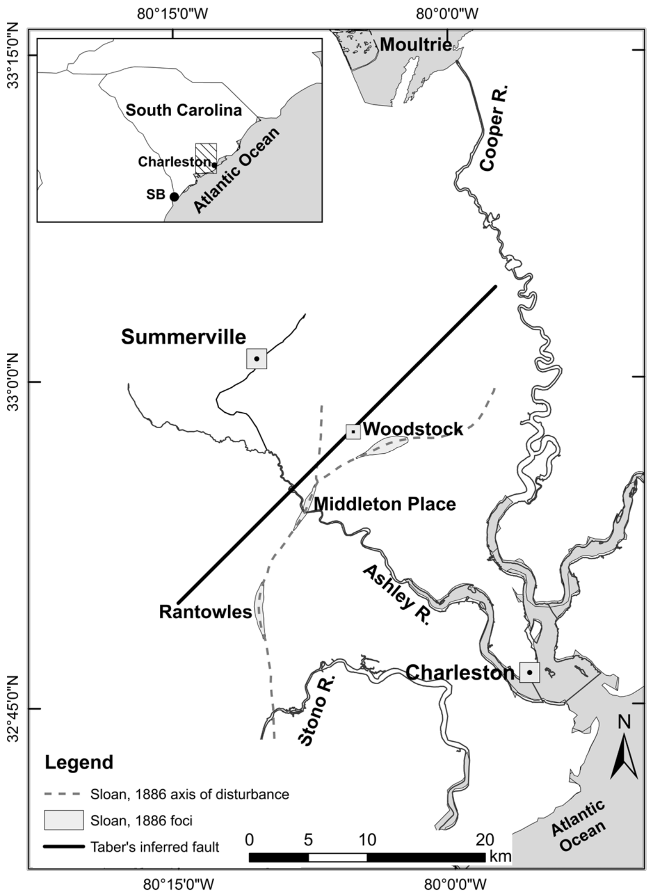

▲ **Figure 1.** The three foci of the 1886 Charleston earthquake (Woodstock, Middleton Place, and Rantowles) according to Sloan (in McKinley 1887). Taber's inferred fault (Taber 1914) for that earthquake is shown with a bold line.

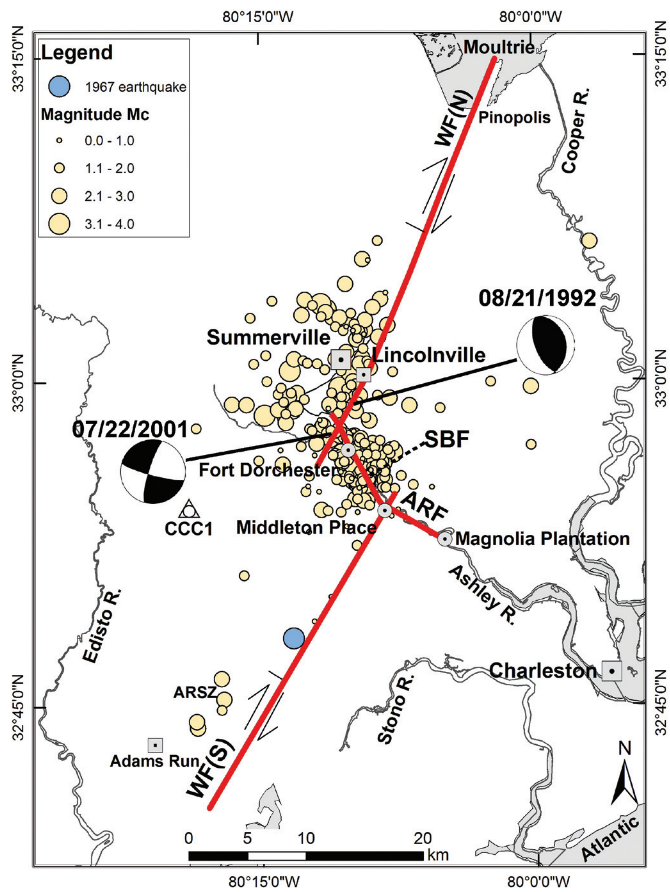

▲ **Figure 2.** Epicentral locations (cream-colored circles) showing A and B quality microearthquakes between 1974 and 2004 and fault plane solutions of the 08/21/1992 **M** 4.1 and the 07/22/2001 **M** 2.3 earthquakes. The dense cluster of seismicity surrounding Fort Dorchester has been named the Middleton Place–Summerville seismic zone (Tarr *et al.* 1981). The blue dot shows the location of the 23 October 1967 **M** 3.4 earthquake (Dewey 1983). The bold red lines show the seismotectonic framework according to Durá-Gómez (2004). The framework consists of the NE trending Woodstock fault (WF), which is cut and offset to the northwest along the Sawmill Branch fault (SBF).

range between M_W 7.3 and 6.9 (Johnston 1996; Bakun and Hopper 2004)

The South Carolina Seismic Network (SCSN) was established in 1974. After analyzing the instrumentally recorded seismicity (1973 to 1979) in the South Carolina Coastal Plain, Tarr *et al.* (1981) defined three clusters of seismicity: Middleton Place–Summerville seismic zone (MPSSZ; Figure 2), the most active; Bowman seismic zone (BSZ); and Adams Run cluster, herein renamed the Adams Run seismic zone (ARSZ). Tarr and Rhea (1983) identified the MPSSZ as the source of the 1886 Charleston earthquake. A variety of fault plane solutions available for the area led Talwani (1982) to consider the possibility of more than one active fault. Talwani (1982) revised the velocity model under MPSSZ, relocated the earthquakes occurring between 1974 and 1980, and defined two faults: the NW-SE trending Ashley River fault (ARF) associated with high-angle reverse faulting and the NNE-SSW trending Woodstock fault (WF, named after Taber's [1914] original suggestion), associated with right-lateral strike-slip movement. He extended the WF southwest to the ARSZ based on the 1967 **M** 3.4 earthquake (Dewey 1983) located between MPSSZ and ARSZ (Figure 2). He inferred a N60°E direction of maximum horizontal compression from the composite fault plane solutions obtained for these earthquakes, later confirmed by Zoback (1983) from studies of well breakout data at the Clubhouse Crossroads deep borehole.

Representative fault plane solutions for two well-located earthquakes, with an epicentral separation of less than 5 km and hypocentral difference of less than 1 km, show remarkably different styles of faulting. The **M** 4.1 event on 21 August 1992 (32.984°N, 80.168°W, 8.0 km) was associated with reverse faulting on a N22°W striking plane, whereas the **M** 2.3 event on 22 July 2001 (32.9587°N, 80.1747°W, 7.0 km) was associated with primarily right-lateral strike-slip on a N17°E striking fault plane (Figure 2). The inferred direction of the *P*-axes for the two fault plane solutions are oriented N70°E and N60°E respectively.

After the identification of two possible faults based on their focal mechanisms and hypocentral distribution (Talwani 1982), subsequent studies further strengthened the observation that multiple faults may be associated with the seismicity in MPSSZ. Shedlock (1987, 1988) revised the earthquake locations from 1974 to 1986 by using a three-dimensional velocity structure. She found hypocenters located as deep as 10 to 12 km in the MPSSZ, with the deeper events located on the west side of the zone and the shallower along the east side of the zone. The fault plane solutions indicated thrust, strike-slip, and normal faulting. She found that the maximum horizontal compressive stress $S_{H\max}$ was oriented NE-SW for events shallower than 9 km and E-W for events from 9 to 12 km deep.

Madabhushi and Talwani (1993) evaluated the instrumental seismicity data from 1980 to 1991. They identified three main groups of earthquakes: the first was associated with the ARF zone (reverse faulting on NW-SE striking, SW dipping fault planes); the second was associated with the WF zone (right-lateral strike-slip motion on NNE-SSW striking vertical faults); and the third was associated with both the ARF and WF zones, suggesting an intersection of these two fault zones.

Garner (1998) re-evaluated the seismicity data from 1974 to 1996 by improving the hypocentral locations and segregating the data into two main groups based on their focal mechanisms and depth distribution. He defined two fault planes: the first, a N10°E striking Woodstock fault, discontinuous, with a left step, offset south of Summerville, along the second fault, the ~NW striking Ashley River fault plane with a ~65° SW dip. Durá-Gómez (2004) reviewed the seismotectonic framework of the MPSSZ. She improved the hypocentral locations from 1974 to 2003 and compared them with the results of various geological and geophysical investigations. Her results indicated that the seismogenic structures are located between 3 km and 12 km in depth and most of the seismicity is located to the northwest of Middleton Place (Figure 2). She divided the originally defined Ashley River fault, extending from the Magnolia Plantation to Summerville, into two parts: a seismically active ~N30°W oriented Sawmill Branch fault (SBF) with a strong reverse component and a dip of about 70° to the southwest, and the ~N50°–60°W, essentially aseismic fault along the Ashley River between Middleton Place and the Magnolia Plantation, for which the name Ashley River fault was retained (Figure 2). Her analysis supported the presence of an offset in the Woodstock fault, with the southern arm oriented ~N30°E and roughly parallel to the northern arm. The strike of the southern arm of WF was based on the seismicity near the Adams Run seismic zone, on the epicenter of the 23 October 1967 **M** 3.4 earthquake obtained by Dewey (1983) and on the focal mechanism of a cluster of events obtained by Talwani (1982). Based on the seismicity, seismic reflection, and geomorphic data, the strike of the Woodstock fault varied from about N30°E to N20°E (Figure 2).

The above observations, different focal mechanisms, and sounds emanating from the epicentral area suggest the presence of multiple faults. Further, most of the nodal planes obtained from the fault plane solutions are not very well constrained (strike uncertainty >15°), and because of the fact that the faults in this area do not have a surface expression, discerning the seismotectonic framework relies on indirect evidence. Both the epicentral (Figure 2) and the hypocentral distributions (Durá-Gómez 2004) do not lend themselves to any obvious division of hypocenters into distinct fault planes. So it was considered necessary to try to further improve the relative locations of the hypocenters using HypoDD (Waldhauser and Ellsworth 2000) before trying to delineate multiple fault planes.

RELOCATION OF EARTHQUAKES USING HYPODD

Seismicity in the MPSSZ is mainly concentrated in a ~30 × 20 km^2 area between Summerville and Middleton Place (Figure 2). Seismic stations of the South Carolina Seismic Network (SCSN; Figure 3) are concentrated around this pocket of seismicity, providing very good azimuthal coverage except for earthquakes located to the north of Summerville (Figure 3). For the period 1974–2004, 294 earthquakes with **M** ≥ 0.4 were located using HYPOELLIPSE (Lahr 1996). These earthquakes were located by using a modification of the 1-D velocity model, originally developed by Talwani (1982) (Table 1). In this model, the depth of the sedimentary section, its *P*-wave velocity, and its *Vp/Vs* ratio (2.93) were obtained from sonic logs in a borehole in the epicentral area. Shallow refraction data (down to 3–4 km) from three reversed profiles were combined with *P*-wave phases for 21 well-located earthquakes and inverted using the program VELEST (Ellsworth 1977) to obtain the velocity model (see Talwani 1982 for details). Station corrections were estimated to account for the differences in the thickness of sediments below different stations. The shallow structure (< 0.7 km) was further confirmed by studying the arrival times for *PS* and *SP* converted phases on three component stations. Small offsets in the basalt layer (< 50 m) below the faults (Paper 2) do not contribute any significant errors in the locations. The *Vp/Vs* ratio used for the lower layers was found to yield the lowest root mean square (RMS) residual values in the earthquake locations. The velocity model was tested by locating blasts used in the refraction surveys. The epicenters were located within 870 m, 555 m, and 385 m of the actual sites (Talwani 1982). Thus, the "absolute" locations obtained by using HYPOELLIPSE are considered to be robust and reliable. Of these, 217 earthquakes were located with quality A and B, with a mean RMS residual of 0.08 s. These correspond to horizontal and vertical location errors of < 1.3 km and < 2.0 km respectively (Lahr 1996). The epicenters of these quality A and B events are shown in Figure 3 together with the focal mechanisms of 17 of the well-located events. This set of 17 well-constrained fault plane solutions with a strike uncertainty ≤ 15° were obtained by using FPFIT and FPPLOT (Reasenberg and Oppenheimer 1985). The focal mechanisms indicate compressional deformation, in agreement with the originally inferred direction of $S_{H\max}$, N60°E (Talwani 1982; Zoback 1983). To further improve the relative locations for tectonic interpretation, we input these 217 events in the double difference (DD) location algorithm HypoDD (Waldhauser 2001).

The DD technique can be applied when the hypocentral separation between two earthquakes is small compared to the

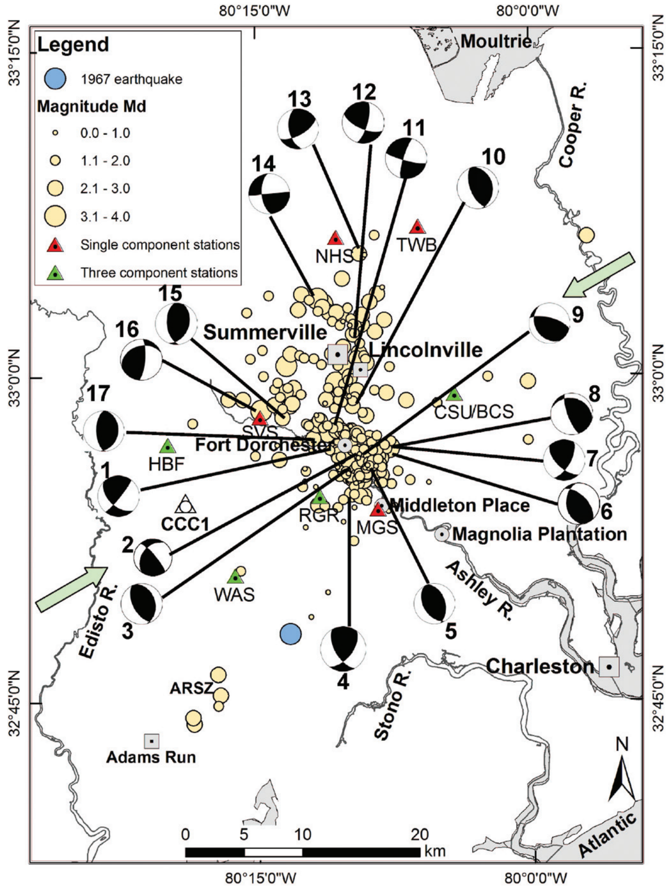

▲ **Figure 3.** Seismicity for the period 1974 to 2004 (quality A and B solutions using HYPOELLIPSE) and 17 well-constrained fault plane solutions (the strike directions are good to ≤15°). All solutions suggest compressional deformation with $S_{H\max}$ oriented N60°E (open arrows). Solutions 1–10 are predominantly associated with NW-SE trending reverse faults and 11–17 with N-S trending strike-slip and reverse faults. Squares and circles with a dot show locations of towns and important landmarks. The epicenters located in the southwestern corner define the Adams Run seismic zone of Tarr *et al.* (1981). The location of the 1967 earthquake was obtained from Dewey (1983).

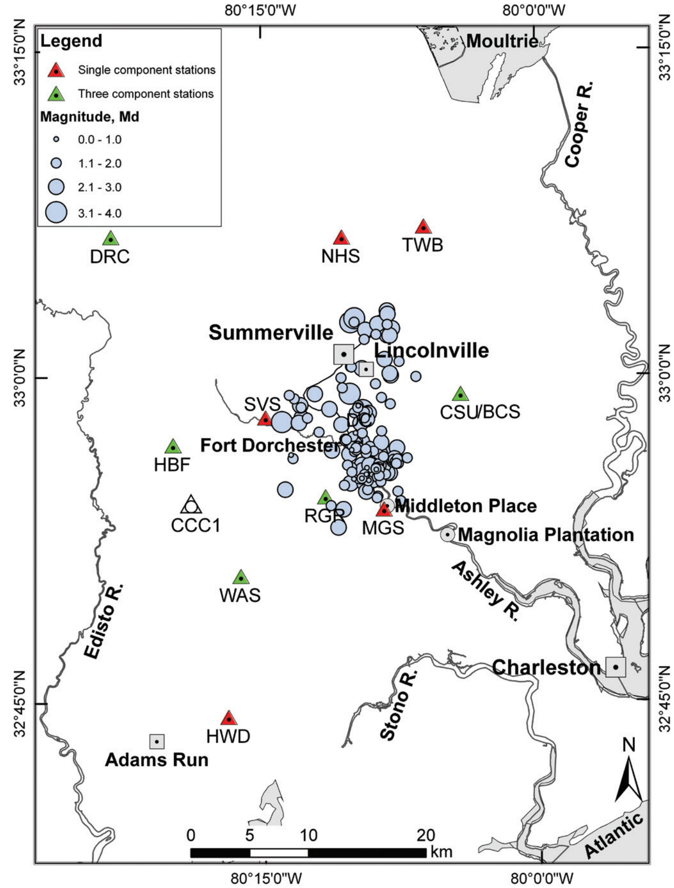

▲ **Figure 4.** Relocated epicentral locations using HypoDD. Note that only about two thirds of the epicenters shown in Figure 3 could be relocated using this method.

distance to common stations and the scale length of velocity heterogeneity in the hypocentral region. In such case, the ray paths are similar and the differences in travel times are mainly due to the spatial offset between earthquakes.

P- and *S*-wave arrival data for 217 events were obtained from the 1974–2004 catalog and were used to obtain the travel-time differences for each event pair, with a separation distance less than 5 km at stations located within 200 km of the cluster centroid. To solve the forward problem, we used the 1-D layered *P* and *S* velocity model (Talwani 1982) shown in Table 1. The HypoDD program that we used did not allow for different *Vp*/*Vs* ratios for different layers. Consequently a *Vp*/*Vs* ratio of 1.71 was used for all the layers (Table 1), in contrast to HYPOELLIPSE where a value of 2.93 was used for the top layer. At the end of the iteration process, a total of 148 events were relocated by HypoDD. The relocated events were grouped into three clusters, the first group consisting of 144 events and the other two consisting of two events each. For the first cluster, we observed a reduction of the average RMS residual from 0.09 s. to 0.02 s and used this for tectonic interpretation. The other clusters contained too few events to yield a meaningful tectonic interpretation. Summarizing, only 144 events from a total of 217 events (66%) in the 1974–2004 catalog were captured by HypoDD with an average RMS residual of 0.02 s. Many of the events rejected by HypoDD because of poor station coverage outside the main cluster had reliable hypocentral HYPOELLIPSE locations. They were, therefore, later used in our analysis to define structures outside the main cluster.

HypoDD is a relative relocation program that is useful in defining seismogenic structures in 3-D. However, it is not nearly as accurate at determining the absolute locations (Waldhauser and Richards 2004) (Figure 4). Therefore, it was considered necessary to use additional data, for example, well-determined hypocenters of larger events and geological, geophysical, and geomorphological data, etc., to constrain the absolute locations (Waldhauser and Richards 2004).

To estimate the expected epicentral displacement of hypocenters (given by HypoDD) with respect to their absolute locations (given by HYPOELLIPSE), we compare these two kinds of locations for 27 earthquakes of magnitude ≥ 2.5.

TABLE 1
Velocity Model Used for Hypocenter Determination*

Vp (km/s)	Depth of top of layer (km)	Vp/Vs
2.20	0.00	2.93
5.50	0.75	1.71
5.60	1.50	1.71
5.75	3.00	1.71
5.90	7.00	1.71
6.45	10.0	1.71
6.70	20.0	1.71
8.15	30.0	1.71

* The above model was used in the program HYPOELLIPSE. For use in HypoDD, a constant *Vp/Vs* ratio of 1.71 was used for all layers.

All these earthquakes were well located by HYPOELLIPSE with RMS ≤ 0.08 s. We found that 23 out of 27 epicenters were displaced with HypoDD less than 2 km from their HYPOELLIPSE location with an average epicentral displacement of about 1.4 km to the southeast (Figure 5 and Table 2). The systematic SE displacement could possibly be because of the incorrect *Vp/Vs* ratio used for the top layer in HypoDD and the paucity of stations to the northwest of the epicentral area (Figure 6). We also calculated the change in their hypocentral depths and found no systematic changes. For 21 of the 27 events the changes in depth ranged between –2.0 and +0.9 km. The largest changes in depths were –3.1 km and +4.3 km. Only the systematic epicentral displacement to the southeast was considered in our seismotectonic interpretation, described later in this paper.

DISCRIMINATION

The revised epicentral locations (Figure 4) do not outline any obvious fault trends, but the various fault plane solutions (Figure 3) suggest that both thrust and strike-slip faults are active in this area. In particular, we note the existence of fault planes oriented primarily NW-SE associated with reverse motion, and also of fault planes oriented N-S associated with both right-lateral strike-slip and reverse motion. From the epicentral locations alone it was not obvious which nodal plane (for the various fault plane solutions) was the fault plane. Therefore, we divided these fault plane solutions into two groups: group I associated with predominantly NW-SE trending faults and group II associated with N-S trending fault planes (Tables 3Aand 3B).

To separate the hypocenters into the different groups we took the following approach. We reasoned that movements on different faults would be associated with different first motions on one or more optimally located seismic stations. To distinguish which earthquakes belonged to which fault planes, we examined the first motions for each earthquake at stations of the SCSN. This was in a search for systematic polarity differences at any station for earthquakes associated with different faults in the same hypocentral region.

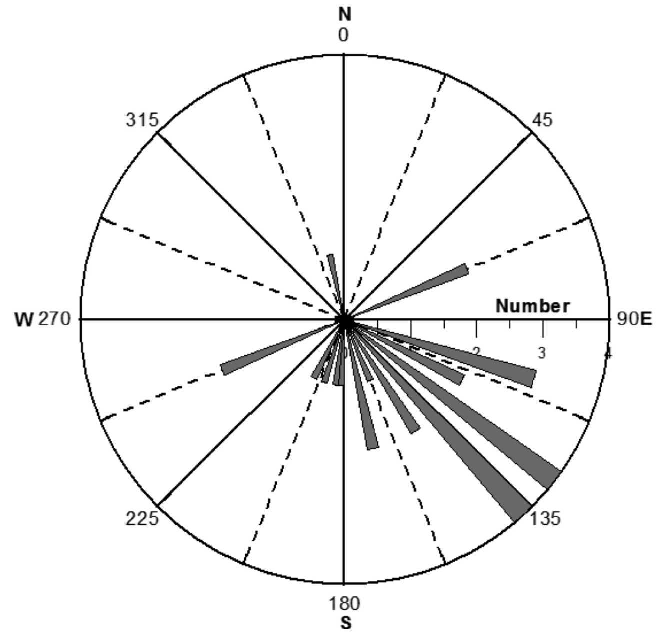

▲ **Figure 5.** Rose diagram showing the angle of displacement from HYPOELLIPSE to HypoDD epicentral locations (measured from the north). The radii give the number of events.

Figure 6(A) shows the locations of the seismic stations that surround the observed seismicity. We considered reliable first-motion data (only picks with a weight of 0 or 1, in computer program HYPOELLIPSE) for all earthquakes at all recording stations. Figure 6(A) shows an outline of the seismically active area (oval) and the locations of the seismic stations. Figure 6(B) shows a histogram of the numbers of events with compressional and dilatational first arrivals by station for all earthquakes listed in the HypoDD catalog. Note that stations BCS (surface sensor), CSU (surface sensor), and CSB (borehole sensor) are essentially at the same location; BCS was moved about 1 km to CSU in 1998. We grouped the arrivals at BCS and CSU (both surface sensors) and denote them as ΣCSU. The number of arrivals at NHS, SGS, and HWD was considered too few to use these stations as discriminants.

To decide which station(s) to use as discriminants, as a first step we analyzed the first-motion data for a set of 17 earthquakes with well-constrained fault plane solutions, which we divided into two groups depending on the inferred strike of their fault planes (Tables 3A and 3B). Our selection of the fault planes was based on the number of solutions along those planes and our current understanding of the seismotectonics of the MPSSZ area (Durá-Gómez 2004; Figure 2). For convenience in the analysis, the compressional and dilatational first arrivals were assigned a numerical value of 1 and 2, respectively. Then, for each station in each group of earthquakes, we calculated the average of the assigned values. For example, for station RGR there were nine events in group I of which five were compressional (designated value 1) and four were dilatational (designated value 2) for an average designated value of 1.4. However, for ΣCSU (sum of CSU and BCS), there were 10 events with an average designated value of 1.9, *i.e.*, predominantly dilatational.

TABLE 2
Hypocentral Changes of Relocated Earthquakes of Magnitude ≥2.5 with Respect to Their Absolute Locations Given by HYPOELLIPSE

Earthquake (year/month/date/hour/min.)	**M** (Magnitude)	**D (km)**	**Angle**	**Δ Depth (km)**
197703300827	2.9	1.9	70°	–3.1
198801230157	3.1	1.3	210°	–1.7
198901021635	2.7	0.9	185°	–1.1
199002070741	2.8	1.6	250°	–1.8
199005111832	2.5	0.8	110°	0.5
199006020257	2.5	1.4	150°	–0.7
199006181003	2.8	1.5	140°	–0.7
199011131522	3.3	0.8	200°	0.2
199108182246	2.9	1.7	190°	–1.7
199205072011	2.5	1.0	70°	3.3
199208211631	4.0	1.5	150°	0.9
199504171346	3.4	1.2	140°	2.5
199711260520	2.5	1.4	170°	0.0
199903291449	3.0	1.4	110°	3.5
200112230557	2.8	1.5	130°	–1.5
200201111330	2.7	2.6	140°	0.8
200207070240	2.9	0.9	250°	–1.7
200207262107	3.0	2.1	110°	4.3
200212160532	2.8	3.0	120°	0.3
200302280702	2.6	1.0	160°	0.0
200303021718	2.9	1.8	150°	0.0
200305051053	3.1	2.4	130°	–1.6
200306122333	2.6	0.8	130°	2.1
200307191422	2.5	0.2	350°	–0.5
200310141045	2.5	0.8	140°	–1.1
200312222350	3.0	0.1	130°	–0.5
200407200913	3.1	1.5	120°	0.6
Average		1.4 km	156°	0.2 km

1. D = Epicentral displacement from HYPOELLIPSE to HypoDD solution
2. Ang = Angle of displacement from HYPOELLIPSE to HypoDD epicentral locations (with respect to north)
3. Δdepth = Change in depth from HYPOELLIPSE to HypoDD epicentral locations (HypoDD-HYPOELLIPSE)

We obtained the average designated values in a similar way for group II (Table 3B). Then we compared the average designated value for a particular station for each of the two groups (Table 3C). If the difference between the average designated values was greater than 0.5 it was used as a diagnostic. Two stations, WAS and ΣCSU, met this criterion. We considered station ΣCSU (sum of CSU and BCS, Figure 7) as our diagnostic station based on the fact that 16 earthquakes were used in obtaining the average value, while only 12 earthquakes were used in the case of WAS. Therefore, we concluded that earthquakes associated with group I (predominantly on NW striking faults) usually had dilatational first arrivals at ΣCSU (average value of 1.9; Table 3A), while earthquakes associated with group II (on N-S oriented faults) had mostly compressional first arrivals at ΣCSU (average value of 1.3; Table 3B). So as a first step while examining all other earthquakes, we used the above criterion to separate the cluster of earthquakes in the MPSSZ into two bins—dilatational first arrivals at ΣCSU, which we associated with reverse movement on NW trending faults; and compressional first arrivals, which we associated with strike-slip on NNE-SSW and N-S trending faults.

We noted that the depths of all the well-located events (using HypoDD) were between 3 and 16 km (Figure 8). Drilling at Clubhouse Crossroads (CCC1 in Figure 6A) encountered basalt flows at a depth of ~0.7 km (Gohn *et al.* 1983) below the pre-Cretaceous unconformity (Ackermann 1983). The three wells at Clubhouse Crossroads were abandoned only a few meters into the basalt and did not penetrate the entire sequence

(A)

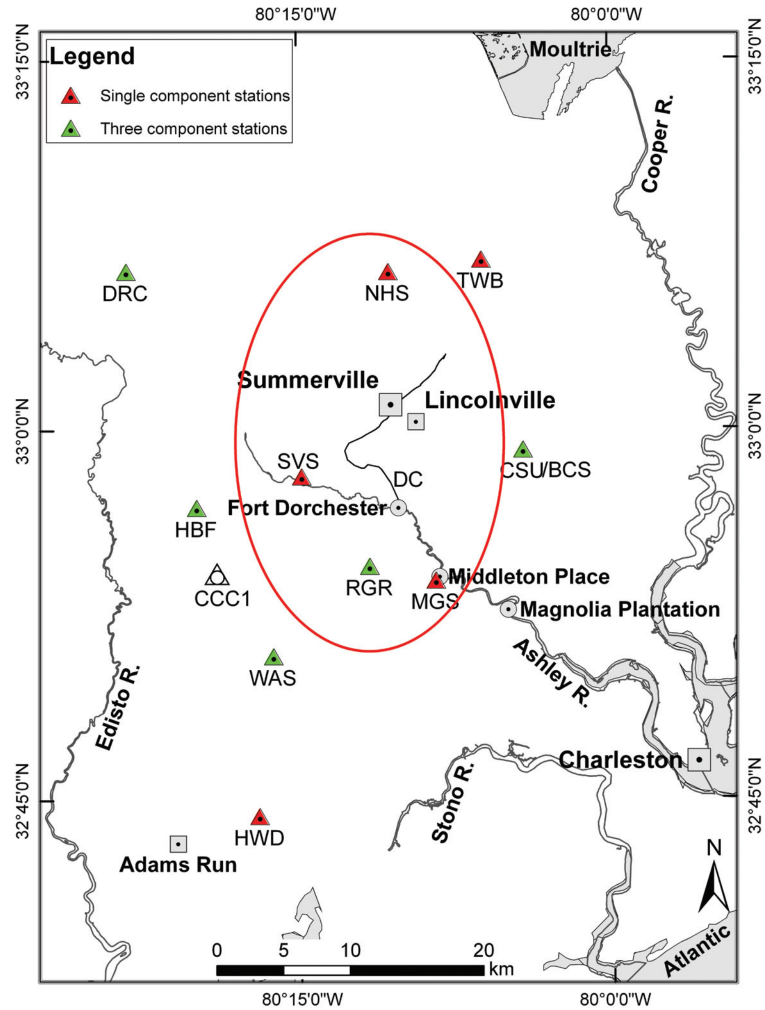

(B)

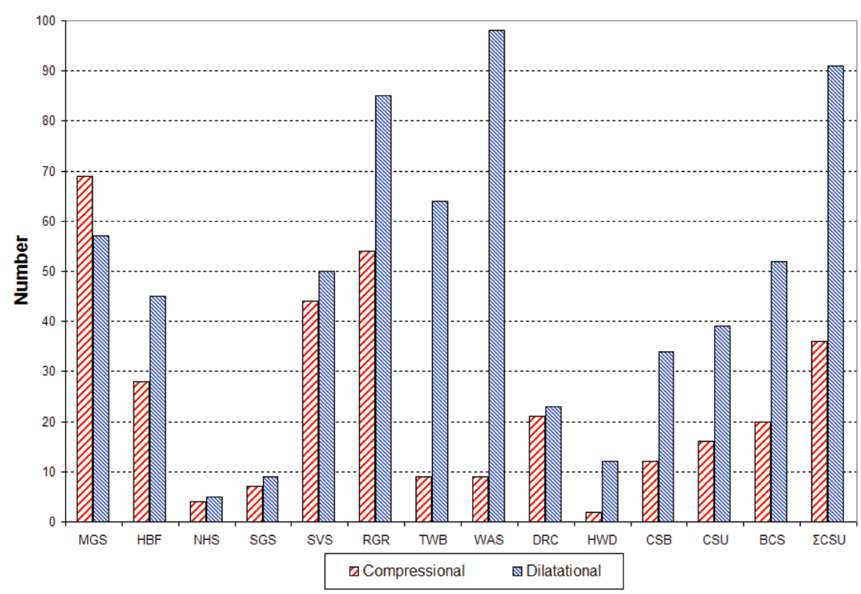

▲ **Figure 6.** (A) Location of seismic stations and boundary of main seismicity area. SGS is located (33.1925°N, 80.5095°W) outside the figure. NHS, TWB, and HWD were deactivated in 1980, 2006, and 1995 respectively. CCC1 shows the location of Clubhouse Crossroads well # 1. DC shows the location of Dorchester Creek; its northeast continuation is called Sawmill Branch. (B) Numbers of compressional and dilatational first arrivals by station for all earthquakes located by HypoDD. ΣCSU is the sum of CSU and BCS.

TABLE 3(A)
Data Pertaining to Fault Plane Solutions of Group I (No Data Available for the Shaded Spaces)

						UP(1) / DOWN(2)							
Event #	**Date**	**M**	**Plane[1]**	**Strike**	**Dip**	**RGR**	**MGS**	**SVS**	**ΣCSU**	**HBF**	**TWB**	**WAS**	**DRC**
1	19910424	1.6	FP	N45°W ± 15°	50° ± 23° (SW)	1	1	2	2	2	1		
			AP	N39°E ± 15°	82° ± 23° (SE)								
2	19831106	3.3	FP	N40°W ± 10°[2]	70° ± 10°[2](NE)		2		1			1	1
			AP	N35°E ± 10°[2]	40° ± 10°[2] (NW)								
3	19890602	2.3	FP	N27°W ± 10°	56° ± 5° (SW)	1	1	1	2	2	2	2	
			AP	N15°W ± 10°	35° ± 5° (NE)								
4	19900207	2.2	FP	N30°W ± 10°	60° ± 10° (SW)	1		2	2	2	1	2	
			AP	N37°E ± 10°	56° ± 10° (SE)								
5	20011223	2.8	FP	N30°W ± 13°	46° ± 23° (SW)	2	1	2	2	2		2	2
			AP	N15°W ± 13°	45° ± 23° (NE)								
6	19901113	2.9	FP	N42°W ± 20°	56° ± 13° (NE)	2	2	2	2		2	2	
			AP	N5°W ± 20°	40° ± 13° (SW)								
7	19910115	2	FP	N45°W ± 15°	60° ± 35° (SW)	2	1	2	2	2	1	2	
			AP	N29°E ± 15°	64° ± 35° (SE)								
8	19881213	2.3	FP	N20°W ± 15°	75° ± 8° (SW)	1		1	2	1			1
			AP	N75°W ± 15°	25° ± 8° (NE)								
9	19971126	2.5	FP	N30°W ± 10°	30° ± 3° (SW)	2	2	2	2	2		2	1
			AP	N74°W ± 10°	67° ± 3° (NE)								
10	19920821	4.1	FP	N22°W ± 5°	59° ± 5° (SW)	1	1	1	2	1	2	2	2
			AP	N10°W ± 5°	26° ± 5° (NE)								
					Average:	1.4	1.4	1.7	1.9	1.7	1.5	1.9	1.4

1. FP: Fault Plane; AP: Auxiliary Plane
2. Estimated

TABLE 3(B)
Data Pertaining to Fault Plane Solutions of Group II (No Data Available for the Shaded Spaces)

						UP(1) / DOWN(2)							
Event #	**Date**	**M**	**Plane[1]**	**Strike**	**Dip**	**RGR**	**MGS**	**SVS**	**ΣCSU**	**HBF**	**TWB**	**WAS**	**DRC**
11	20010722	2.3	FP	N17°E ± 8°	80° ± 13° (NW)	2	1	2	2	2	2		
			AP	N75°W ± 8°	80° ± 13° (SW)								
12	20000507	1.3	FP	N16°E ± 5°	72° ± 20° (SE)		1	2	1	2	2		2
			AP	N65°W ± 5°	65° ± 20° (SW)								
13	19980911	2.1	FP	N10°W ± 3°	54° ± 10° (SW)	1	2	1		1	2	1	2
			AP	N60°E ± 3°	65° ± 10° (SE)								
14	20020726	3	FP	N5°W ± 3°	60° ± 10° (W)	2	1	2	1	2	2	2	1
			AP	N85°W ± 3°	90° ± 10° (S)								
15	20001019	2	FP	N20°E ± 10°	40° ± 5° (SE)	1	2	1	1	2	2	1	2
			AP	N5°W ± 10°	53° ± 5° (W)								
16	20040720	3.1	FP	N20°E ± 5°	70° ± 5° (SE)	1		1	1	2		1	2
			AP	N48°E ± 5°	22° ± 5° (NW)								
17	19991101	2.4	FP	N10°E ± 8°	30° ± 0° (SE)	1	2	1	2	2	2		2
			AP	N2°W ± 8°	61° ± 0° (W)								
					Average:	1.3	1.5	1.4	1.3	1.9	2.0	1.3	1.8

1. FP: Fault Plane; AP: Auxiliary Plane
2. Estimated

Table 3C: Comparison of results for Group I and Group II				
	Average Designated value*			Number of Earthquakes Considered
	Group I	Group II	Difference	
RGR	1.4	1.3	0.1	15
MGS	1.4	1.5	0.1	14
SVS	1.7	1.4	0.3	16
ΣCSU	1.9	1.3	0.6	16
HBF	1.7	1.9	0.2	16
TWB	1.5	2.0	0.5	12
WAS	1.9	1.3	0.6	12
DRC	1.4	1.8	0.4	11

of basalt flows. However, a speculative well (in search of oil and gas) drilled at Lodge (33° 00′ 54″ N, 80° 55′ 44″ W) encountered basalt at depth of 1.4 km. It was drilled to a total depth of 3.8 km and bottomed out in basalt (Talwani 2000, unpublished data) suggesting that the basalt extended to a greater depth. The crystalline basement lies below the layer of basalt flows and intercalated sediments. In the MPSSZ, based on the seismic refraction velocities, Ackermann (1983) interpreted the top of the crystalline basement to be located between 1,200 m and 2,400 m. We interpret the hypocentral depths at MPSSZ (≥ 3 km) to suggest that the earthquakes are occurring along faults below the basalt and in the crystalline basement.

Figure 7 shows the epicentral locations of events located by HypoDD, segregated by their first arrivals at ΣCSU. Since HypoDD locations did not include epicenters north of Summerville because of inadequate station coverage to the north, we included well-located events (HYPOELLIPSE) in that area (stars) for which the first arrival was primarily compressional to better identify the WF. Note that the relative epicentral locations obtained by HypoDD are offset ~1.4 km to the southeast compared to those obtained by HYPOELLIPSE (stars). For tectonic interpretation, the relative locations obtained from HypoDD were moved 1.4 km to the northwest and merged with the absolute locations from HYPOELLIPSE. We note that the most intense seismicity occurs in the vicinity of Fort Dorchester and Middleton Place. In this area epicenters with both dilatational and compressional first arrivals at ΣCSU are present, suggesting the presence of two or more styles of faulting, although dilatational arrivals are predominant. To the north of Fort Dorchester, the seismicity is less dense; however, epicenters with both compressional and dilatational first arrivals at ΣCSU are present (Figure 9).

We plotted these earthquakes in cross-sections to study their three-dimensional configuration. The hypocenters were viewed in 3-D using the ArcScene visualization tool of ArcGIS (ESRI Inc.; http://www.esri.com/arcgis). The directions of the cross-sections were chosen based on the 3-D configuration of the hypocenters and other supporting geomorphic and/or geophysical data. All earthquakes with dilatational first arrivals at ΣCSU (solid circles, Figure 7) were plotted along a cross-section

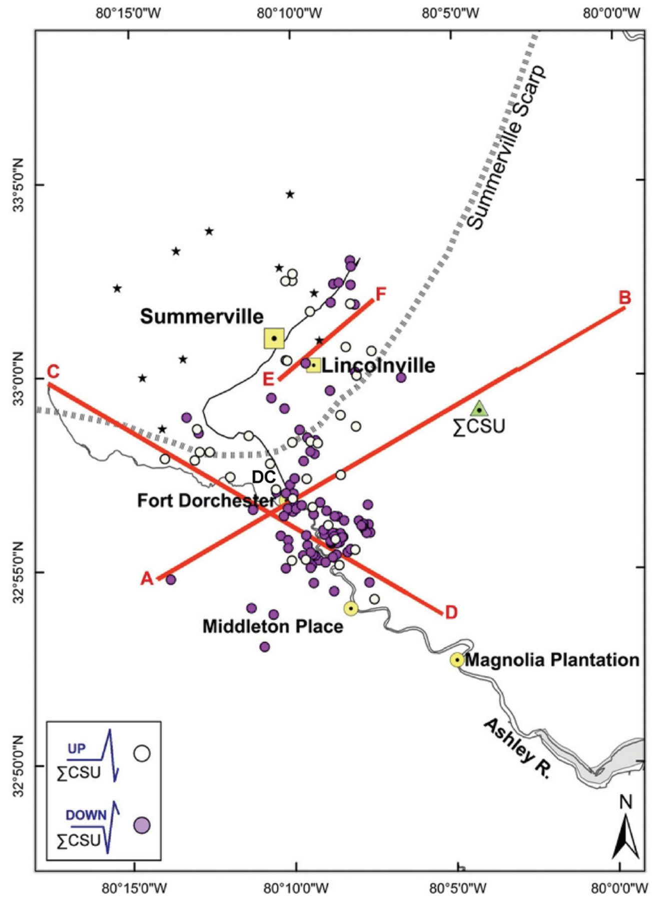

▲ **Figure 7.** Epicentral locations obtained from HypoDD. Earthquakes with compressional and dilatational first arrivals at ΣCSU are shown by open and solid circles, respectively. A and B quality locations of events obtained by HYPOELLIPSE north of the Summerville scarp are shown by stars. DC shows the location of Dorchester Creek. Cross-sections were obtained along AB, CD, and EF (see text for details).

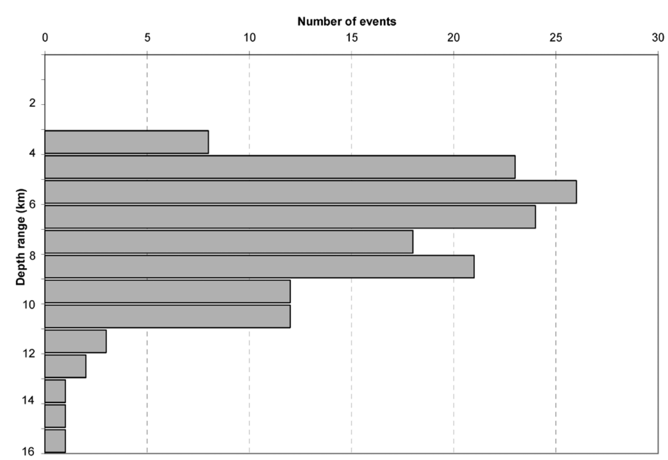

▲ **Figure 8.** Depth distribution of earthquakes (using HypoDD). Most of the hypocenters lie between 3 and 13 km depth.

AB consistent with the 3-D views of hypocenters (Figure 10) drawn perpendicular to Dorchester Creek (DC in Figure 7). The location of the Dorchester Creek was inferred to be fault-controlled based on its geomorphic configuration. In this cross-section, we notice two clusters of seismicity separated by about 5 km along with a few outliers. Most of the earthquakes in the southwestern cluster (shown in red in Figure 10) lie within ~2.5 km of Dorchester Creek and its southeast extension up to Middleton Place, at depths of about 3 km and 13 km, and define a broad zone of seismicity. We have named it the Sawmill Branch fault zone (SBFZ) because of the overlying Sawmill Branch–Dorchester Creek (DC in Figure 7). We interpret the configuration of the SBFZ seismicity in two different but possible ways. The first is a broad zone dipping about 70° to the southwest (Figure 10A); the second is a series of parallel faults dipping steeply to the northeast (Figure 10B). Of these two interpretations we prefer the latter based on mechanical arguments that are described in the next section. The northeastern cluster (shown in blue in Figure 10) defines a narrow SW dipping zone with depths between ~6 km and 12 km. If this zone is extended to the surface, it lies roughly near the surface location of the NW-SE trending Charleston fault (CF), mapped by shallow drilling (Colquhoun *et al.* 1983; Lennon 1985; Weems and Lewis 2002) (Figure 10A). The hypocenters are inadequate to accurately constrain the dip of CF. Using shallow stratigraphic data that defined the presence of Mount Holly dome (Weems and Lewis 2002 and Paper 2), we estimate a dip of about 40° for CF.

We plotted all the earthquakes located by HypoDD with compressional first arrivals at ΣCSU (Figure 7) along a cross-section CD. Seismic reflection surveys (Hamilton *et al.* 1983; Marple 1994) had mapped a NE trending fault in the basalt layer at a depth of 700 m under the Coastal Plain sediments. This fault was identified as Woodstock fault (north) [WF(N)] (Durá-Gómez 2004), and cross-section CD, trending N60°W to S60°E, was chosen perpendicular to this Woodstock fault (Figure 11). We note that the hypocenters define a NW dipping plane.

A number of earthquakes in the Summerville area (northern area of MPSSZ) were not included in the final solution given by HypoDD due to the poorer station coverage of these events. Because they were well located (quality A and B solutions using HYPOELLIPSE), they are included here in our tectonic evaluations. These ten events, with compressional first arrivals at ΣCSU, are shown by stars in Figure 7. We note that the epicenters of the earthquakes with compressional first arrivals at ΣCSU lie in two broad zones: one to the north of Fort Dorchester and the other to its southeast. These additional ten events were added to the cross-section along CD and are shown by squares in Figure 12A. In this cross-section, to compare with the absolute locations obtained from HYPOELLIPSE, the relative locations obtained from HypoDD were moved 1.4 km (see Table 2) to the northwest (Figure 12A). Of these 10 events, four, shown by green squares, seem to define an additional plane dipping to the northwest, whereas the other six, shown by pink squares, lie to the northwest. The epicentral locations of the events comprising the NW dipping planes are shown in Figure 9. Those epicenters that lie to the north of the Ashley River and have been associated with WF(N) are shown in green in both Figures 12A and 9. Another set of hypocenters (shown in yellow in Figures 12A and 9) lying to the southeast of WF(N) outlines the Woodstock fault (south), WF(S). The two are offset ~6 km at the surface and converge at depth. These data suggest a northwestern dip of about 50° for WF(S) and a steeper dip for WF(N).

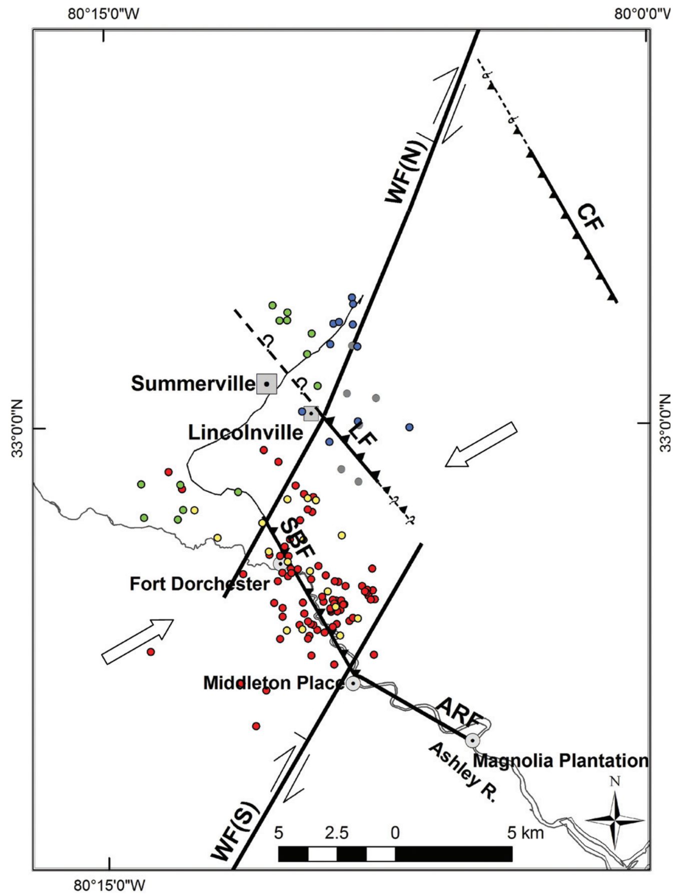

▲ **Figure 9.** Close-up view of the revised seismotectonic framework based on the analysis of seismological data showing the inferred faults and the earthquakes used to define them. The epicentral locations of the earthquakes are color-coordinated with the different faults interpreted here and in the cross sections (Figures 10–13). They are WF(S) (yellow), WF(N) (green), SBF (red), CF (blue), and LF (gray). For the epicenters shown in red and blue the first arrival at CSU was down, and for those shown in gray, green, and yellow, it was up. Open arrows show the $S_{H\max}$ direction, N60°E. The figure shows the most prominent styles of faulting.

Northwest and southeast of the line marked EF in Figure 7, we note a broad NW-SE trend of epicenters with compressional first arrivals at ΣCSU (open dots in Figure 7). This trend is also apparent in the original locations obtained by using HYPOELLIPSE (Figure 3). We interpret these observations to suggest the possible existence of another NW-SE trending fault plane. However, seven of these earthquakes, including

(A)

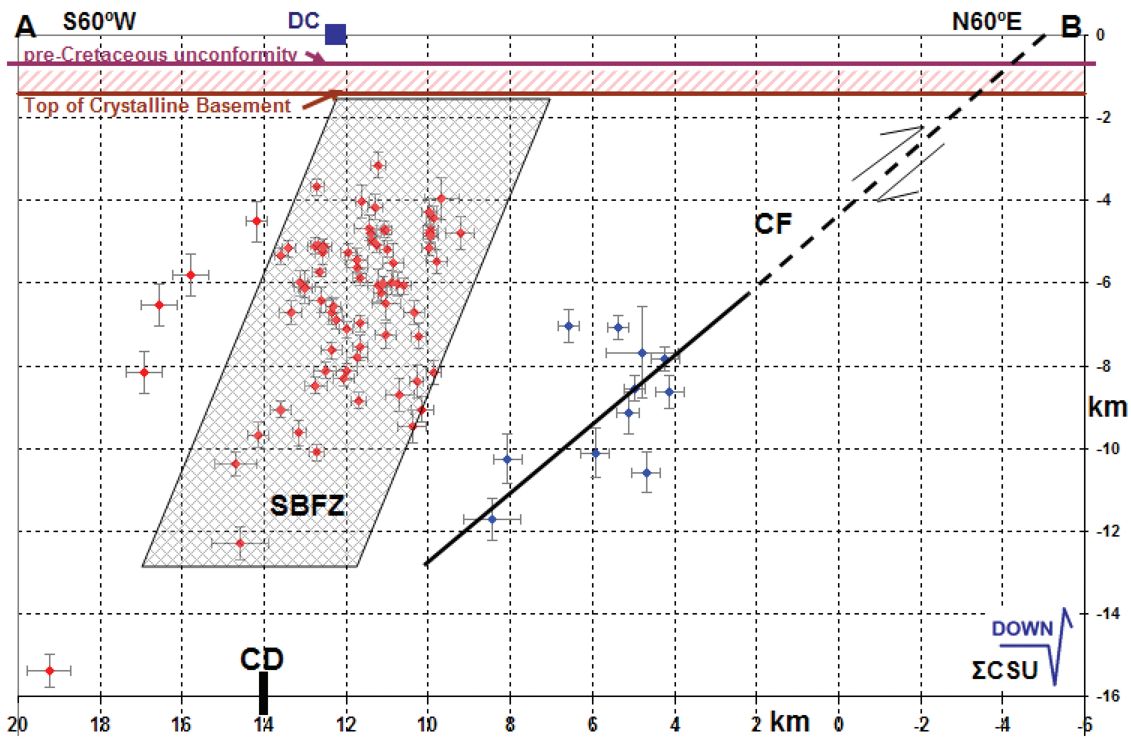

(B`)

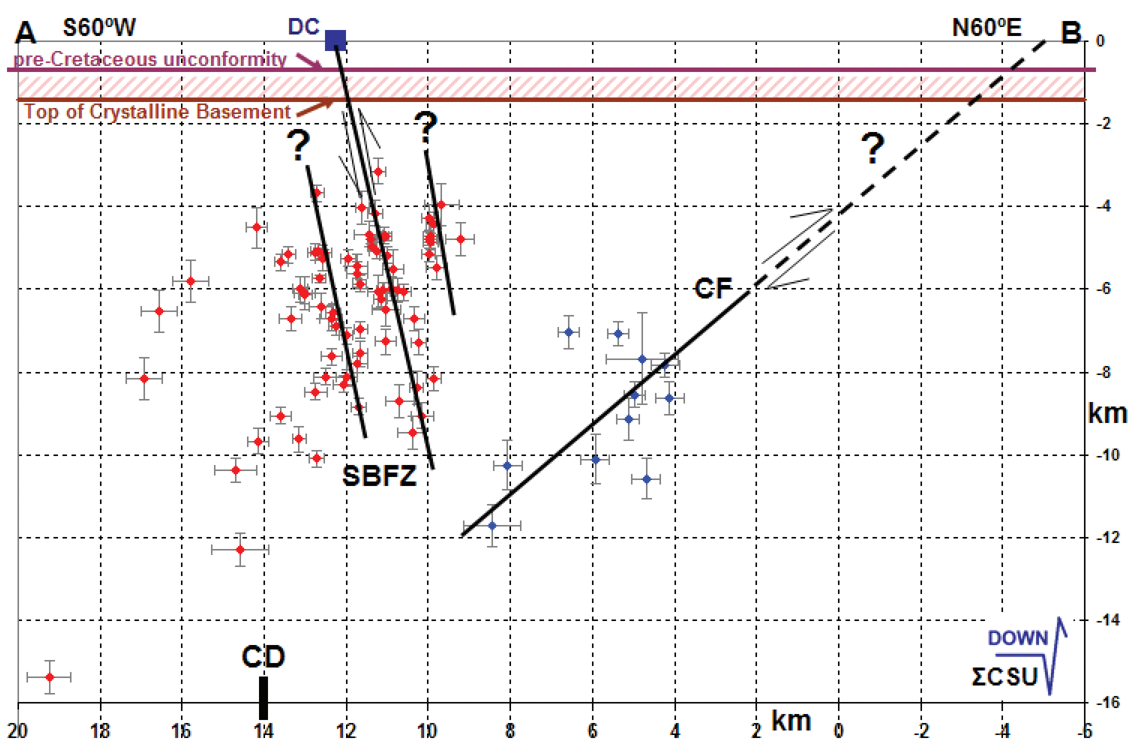

▲ **Figure 10.** (A) Cross-section along AB (Figure 7) oriented S60°W-N60°E showing earthquakes with dilatational first arrivals at ΣCSU (solid circles in Figure 7), which define the Sawmill Branch fault zone (SBFZ) and the Charleston fault (CF). The shaded area in red shows the interpreted location of basalt flows and intercalated sediments. A preliminary interpretation suggests a ~70° SW dip for SBFZ and a ~40° SW dip for CF. DC (blue square) on the surface shows the location of Dorchester Creek. CD shows where the cross-section along CD intersects the present cross-section. (B) An alternate interpretation of the cross-section along AB suggests the presence of a series of parallel faults in the SBFZ dipping steeply to the northeast, while the CF dips ~40° to the southwest. The shaded area in red shows the interpreted location of basalt flows and intercalated sediments. DC (blue square) on the surface shows the location of Dorchester Creek. CD shows where the cross-section along CD intersects the present cross-section.

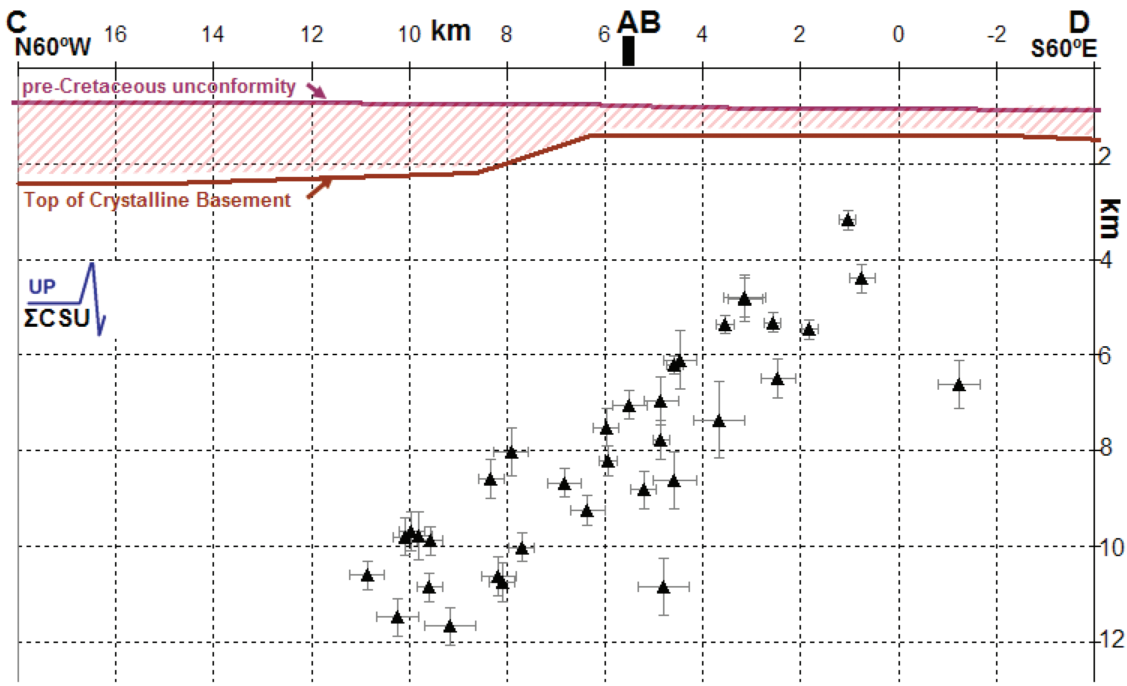

▲ **Figure 11.** Cross-section along CD (Figure 7) oriented N60°W-S60°E, showing only compressional arrivals at ΣCSU (open circles in Figure 7). The shaded area is the inferred location of basalt flows and intercalated sediments. AB shows where the cross-section along AB intersects the present cross-section.

three events well located by HYPOELLIPSE but not located by HypoDD, were used earlier in defining WF(N) and are shown by green dots in Figure 9. Removing these events from the cross-section along CD (Figure 12B) and including them instead in a cross-section along EF (Figure 13A) suggests the presence of a steep (~80°) NE dipping fault, which we have named the Lincolnville fault (LF in Figure 9). However, if we retain these events in Figure 12A, the few remaining hypocenters in a cross-section along EF (Figure 13B) are inadequate to clearly define any fault plane. Nevertheless the 3-D view suggests that they are possibly associated with two NE dipping planes. So we note that while Figures 12A and 13B support the presence of WF(N), Figures 13A and 12B suggest the presence of LF. The seismicity data alone cannot distinguish between these interpretations or rule out the presence of both faults. To distinguish between these possibilities we had to incorporate additional geological and geophysical data (Paper 2).

Our revised tectonic framework in the Middleton Place–Summerville area is shown in Figure 9. The epicenters are shown in the same colors as in the cross-sections (Figures 10–13). We combined the dips obtained from the cross-sections with other data to project the faults to the surface. For the WF(N) we took its location at a depth of ~700m, inferred from the seismic reflection data, and a dip of ~50° to obtain its location at the surface. We took the surface projection of the seismicity (Figure 10B) to define the SBFZ. We used the linear portion of the Dorchester Creek (from ~32° 57.926′ N, 80° 10.6625′ W) and extending southeast along the Ashley River to Middleton Place to represent the surface expression of the main segment of the SBFZ and to define its lateral extent. For the strike and extent of the WF(S), we followed the configuration given by Durá-Gómez (2004). That was based on the 3-D configuration of the seismicity near Middleton Place and to the southwest up to the Adams Run seismic zone and on the location of the **M** 3.4 earthquake on 23 October 1967 by Dewey (1983; Figure 2). This configuration is supported by a variety of other data, which are described in Paper 2. For the CF and LF we took their surface locations from surface projections of the seismicity shown in the cross-sections of Figures 10B and 13A. The aseismic ARF, which lies along the Ashley River between Middleton Place and the Magnolia Plantation, lies outside the seismotectonic framework containing the faults associated with the current seismicity. Based on the focal mechanisms (Talwani 1982; Madabhushi and Talwani 1993; Garner 1998; Durá-Gómez 2004; this study), and the WF(N and S) faults are associated with right-lateral oblique strike-slip motion, while the NW-SE trending faults, steeply dipping in the SBFZ and LF and shallowly dipping CF, are associated with oblique left-lateral strike-slip and reverse faulting in response to an in-situ stress field with the direction of the maximum horizontal stress field oriented N60°E (Figure 9).

CONCLUSIONS

Macroscopic observations following the 1886 Charleston earthquake, and analysis of seismicity data between 1974 and 2004 (*e.g.* Talwani 1982; Madabhushi and Talwani 1993; Garner 1998; Talwani 2001; Durá-Gómez 2004) suggest that there are two or more active fault planes in the Middleton Place–Summerville seismic zone undergoing compressional

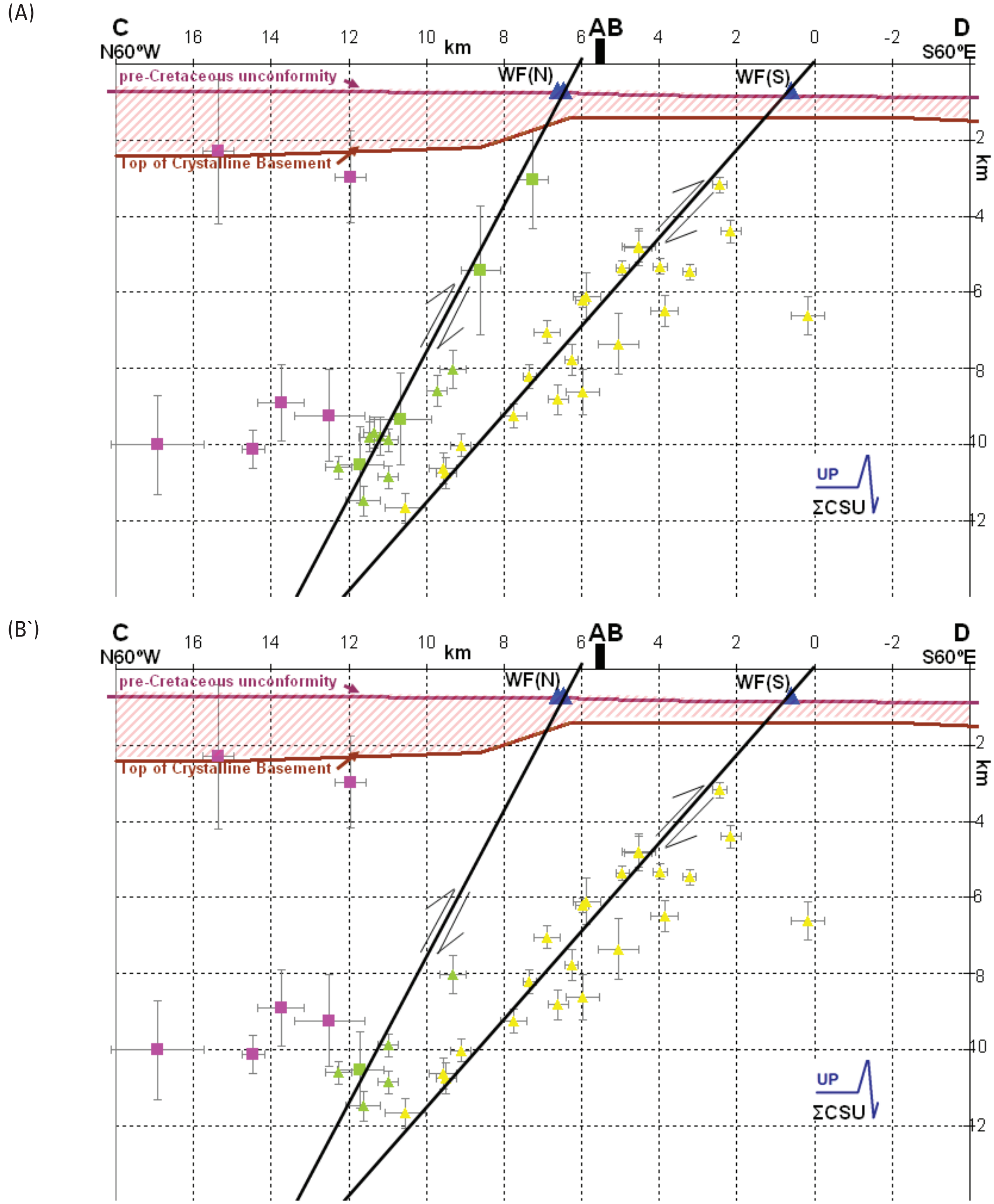

▲ **Figure 12.** (A) Cross-section along CD (Figure 7) showing earthquakes with compressional first arrival at ΣCSU. Earthquakes located by using HypoDD and A and B quality hypocentral locations obtained with HYPOELLIPSE are shown by triangles and squares respectively. The colors are coordinated with their epicentral locations shown in Figure 9. Earthquakes associated with WF(N), green, lie to the north and west of the Ashley River, whereas those with WF(S), yellow, lie along the Ashley River and to the south. Earthquakes located using HypoDD have been translated 1.4 km to the northwest to compare with the absolute locations given by HYPOELLIPSE and supplementary data. The shaded area shows the interpreted location of basalt flows and intercalated sediments. The faults mapped in the basalt are shown as blue triangles. This and other complementary data suggest that the surface expression of the WF(S) is located at ~(0, 0) km while the surface expression of WF(N) is located at ~(6.3, 0) km. WF(S) dips about 50° to the northwest. The inferred location of both WF(S) and WF(N) at the surface is in agreement with corroborative data on the basalt flows (700 m depth) and surface geology (see companion paper). The dip of WF(N) is not well constrained. AB shows where the cross-section along AB intersects the present cross-section. (B) Resulting cross-section along EF after the removal of the seven earthquakes in Figure 12(A) that are included in Figure 13(A) (in green) to define the Lincolnville fault (LF).

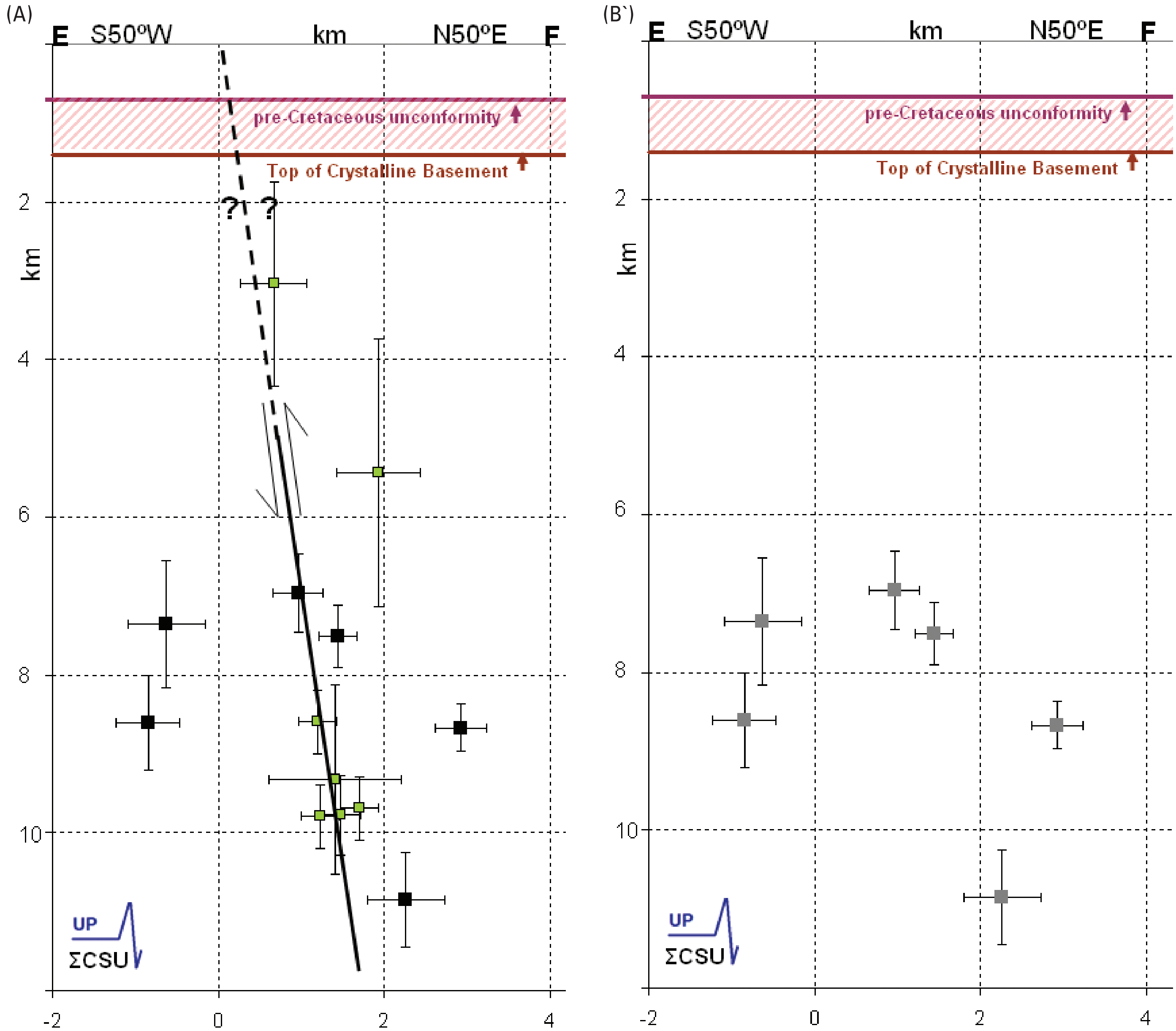

▲ **Figure 13.** (A) Cross-section along EF (map view in Figure 7 and shown in gray and green in Figure 9). Earthquakes that were used to interpret the WF(N) (Figure 12A) are shown in green. Hypocentral locations suggest a steep (~80°) NE dipping fault, which we have named the Lincolnville fault (LF). The shaded area shows the interpreted location of basalt flows and intercalated sediments. (B) Cross-section along EF (map view in Figure 7 and shown in green in Figure 9). The earthquakes that were used to describe the WF(N) in Figure 12A have been removed. The remaining hypocentral locations are too few to define a fault plane(s). The shaded area shows the interpreted location of basalt flows and intercalated sediments.

deformation in response to a stress field with the direction of the maximum horizontal stress ($S_{H\max}$) oriented ~N60°E. We used the polarity of the first arrivals at ΣCSU and suitably oriented cross-sections using revised hypocenters obtained by HypoDD to obtain a revised seismotectonic framework and identify the fault planes on which the seismicity is occurring. The results of these studies suggested the presence of a major NE-SW strike-slip fault system (WF), with NW-SE trending thrust fault(s) near Middleton Place. The geometry and the nature of these faults were not previously well defined.

The revised framework consists of the N30°E oriented Woodstock fault (WF), associated with oblique right-lateral strike-slip motion, which because of its length was probably associated with the mainshock of the 1886 Charleston earthquake. WF has an antidilatational compressional left step near Middleton Place, which divides it into two parts, WF(N) and WF(S), both of which dip steeply (≥ 50°) to the northwest. The seismicity along these faults lies between depths of 3 and 12 km. WF(N) and WF(S) are separated by ~6 km at the surface (at the left step) and converge at depth. Most of the current micro-

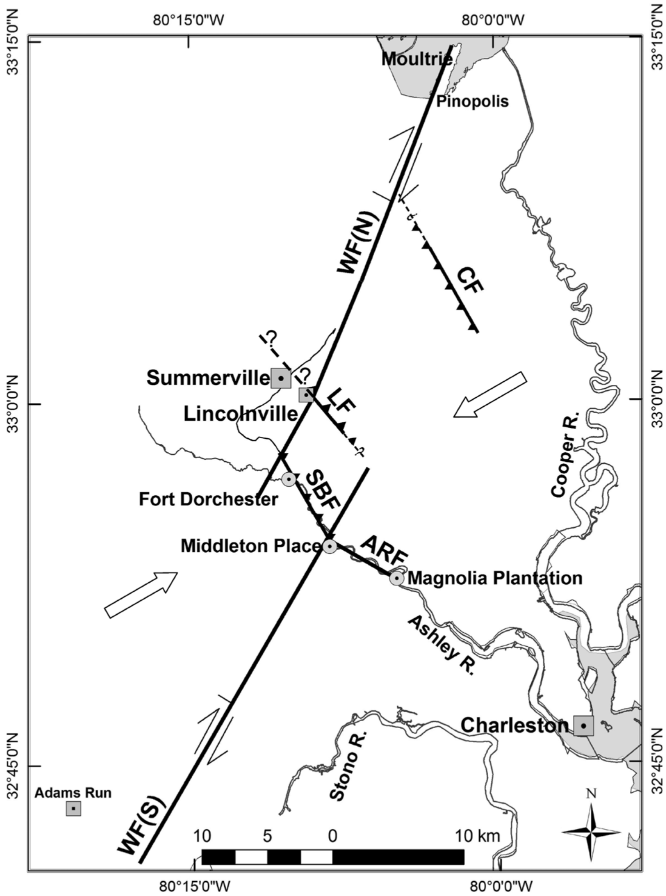

▲ **Figure 14.** The revised seismotectonic framework. WF(N) continues northeast to Pinopolis, and WF(S) continues southeast to the Adams Run seismic zone near a town by that name.

earthquake activity is occurring along three roughly parallel N30°W to N40°W striking faults located within the left step. These NW-SE striking faults are oriented at about ~60° to 70° to WF. The most active of these is the ~3 to 4 km broad, diffuse, Sawmill Branch fault zone (SBFZ) which offsets the WF near Middleton Place. About 5 km and 18 km northeast of SBFZ lie the Lincolnville and Charleston faults (LF and CF), respectively. LF dips steeply to the northeast whereas CF dips shallowly to the southwest, and seismicity on these faults lies between depths of 3 and 12 km. Fault plane solutions for events in the SBFZ suggest reverse faulting on SW or NE dipping fault planes (events 3, 5, and 6 in Figure 3) or reverse faulting with left-lateral strike-slip motion on them (events 1, 2, 7, and 9 in Figure 3).

Our analysis using new and improved relocations using HypoDD suggests two possible geometric configurations for the broad SBFZ. The first is a broad SW dipping fault plane (Figure 10A), and the second is a diffuse zone consisting of subparallel steep NE dipping faults, which together comprise the SBFZ (Figure 10B). We favor the latter interpretation, which together with the NE dip of the LF and SW dip of the CF (Figure 14) is compatible with sand box models of restraining step-overs in strike-slip fault systems (McClay and Bonora 2001), with the theoretical analysis by Segall and Pollard (1980), and with the analysis of antidilatational jogs by Sibson (1986). Segall and Pollard (1980) suggested that, for left-stepping cracks, the mean stress is everywhere compressive and that the compression increases above the background value in the region between the cracks, while in the region outside the cracks the mean stress is less than the background value. For a driving stress increased above the frictional resistance to slip, left-lateral secondary shear fractures may form within the step oriented at about 60° to the lengthened segments (Segall and Pollard 1980). In our case, the SBF, LF, and CF lie at angles of about 60° to 70° to WF(N) and WF(S). Additionally, fault plane solutions suggest that the SBF behaves as a left-lateral fracture but also displays a significant reverse component.

The revised tectonic framework for the MPSSZ proposed in this paper is different from earlier interpretations in the following ways: (a) The seismicity in the MPSSZ is associated with a major strike-slip fault system (WF(S) and (N)) with an antidilatational left step at Middleton Place. Three short NW-SE trending faults lie within this left step and, together with WF(N) and (S), are the location of a localized stressed volume and the observed seismicity. This interpretation differs from our earlier interpretation where the seismicity was associated with fault intersections. (b) The inferred dip direction of the SBF (NE) is opposite to the earlier interpretation of a SW dip for it (Durá-Gómez 2004) and the Ashley River fault (Talwani 1982; Madhabhushi and Talwani 1993; Garner 1998). (c) The ARF, originally interpreted as a NW trending fault, extending from the Magnolia Plantation to Summerville, is now interpreted to be two faults. They are the seismically active SBF, lying within the step over and trending N30°W from Middleton Place and the aseismic ARF, trending ~S55°E from Middleton Place to the Magnolia Plantation.

We compare our seismotectonic model with the analysis by Sibson (1986) and the seismicity pattern following the 1968 Borrego Mountain earthquake (Figure 15). In Sibson's analysis, the left-stepping antidilatational jog (Figure 15B) forms potential locking points, and slip transfer is accompanied by widespread subsidiary faulting. This faulting located in the left step consists of roughly parallel reverse faults that face each other (Figure 15B). He also found that seismicity was not confined within the left step but also occurred outside it. In our case, the MPSSZ (Figure 15A) mimics the seismicity pattern suggested by Sibson (1986). If we consider the SBFZ to consist of parallel NE dipping faults (Figure 10B) and with the CF dipping to the SW, the patterns and dips of the reverse faults observed within the left step closely resemble those suggested by Sibson (1986) (Figure 15B).

This pattern of strike-slip faulting on a main fault near a left step antidilatational jog followed by reverse faulting on faults within the jog was observed in the **M** 6.4 1968 Borrego Mountain earthquake sequence (Figure 15C). The mainshock was associated with right-lateral strike-slip on a NW striking fault plane and was followed by a left-lateral strike-slip event on the main fault and a reverse faulting on the cross faults within the left step (Burdick and Mellman 1976). Our seismotectonic framework for MPSSZ is compatible with the results from sand box experiments (McClay and Bonora 2001) and with the

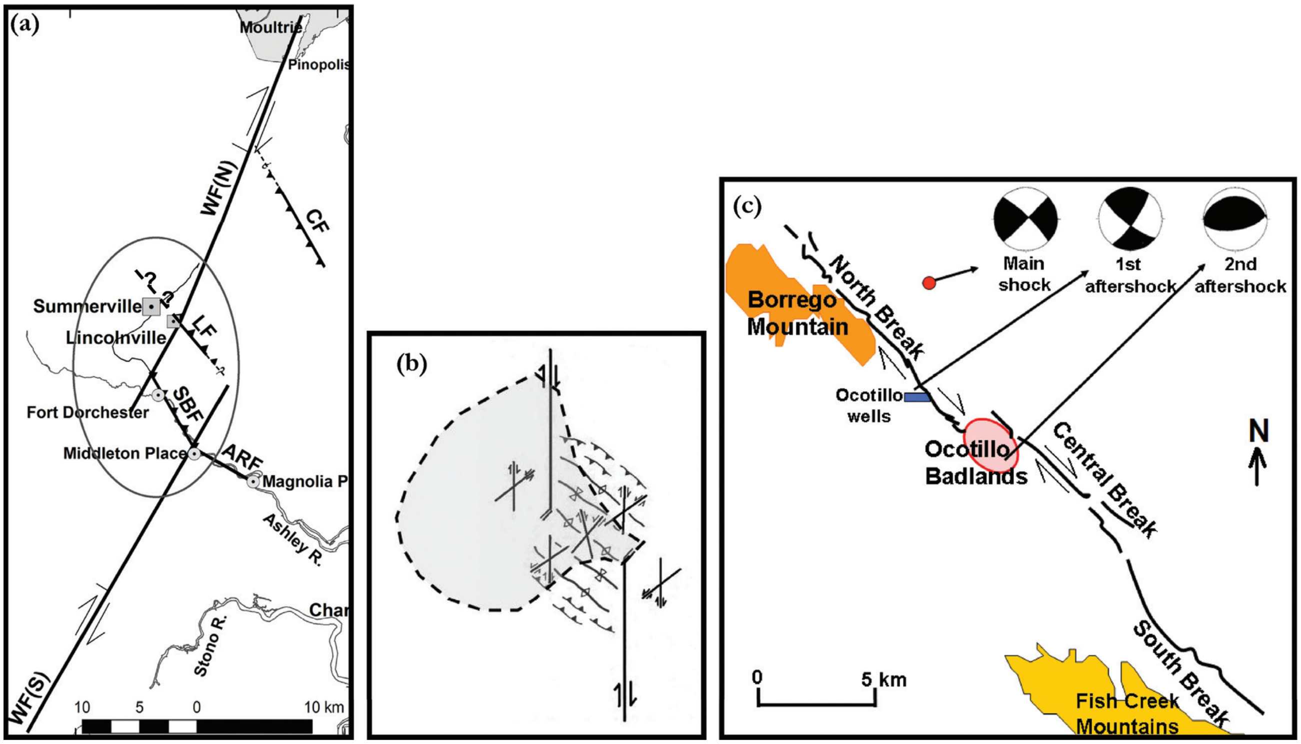

▲ **Figure 15.** Comparison of the (A) seismotectonic framework of the MPSSZ with (B) the analysis of Sibson (1986) for antidilatational jogs and (C) the style of faulting of the 1968 Borrego Mountain earthquake and its aftershocks, modified from Burford (1968) and Burdick and Mellman (1976). The ellipse in (A) shows the boundary of the MPSSZ seismogenic area. In antidilatational jogs Sibson reports compression associated with folds and thrusts, as well as large aftershock distributions (shaded area). Our interpretation of the seismotectonic framework for MPSSZ, a right-lateral strike-slip fault with a left step associated with a series of steeply dipping reverse faults with opposing dips, agrees with the analysis of Sibson (1986) for the style of faults with an antidilatational left-stepping jog. The style of faulting at Charleston, right-lateral on WF and (primarily) reverse on SBF, is similar to that observed from the Borrego Mountain earthquake.

analysis of antidilatational jogs by Sibson (1986) and the faulting observed in the Borrego Mountain earthquake sequence.

In the seismotectonic framework presented in this paper, we note that the seismicity in MPSSZ occurs along different faults and by different mechanisms. These faults lie deeper than ~3km, *i.e.*, below the Coastal Plain sediments and the extensive basalt flows. Movements on these faults affected the overlying basalt flows and sediments, and they accounted for the different macroscopic effects described earlier in this paper. Both the sand box experiments (McClay and Bonora 2001) and Sibson's (1986) analysis predict localized uplift between the SBFZ and CF.

To test the validity of our model of the seismotectonic framework, we compare these locations of the faults and inferred movements on them with a variety of complementary data in the companion paper (Talwani and Durá-Gómez 2009).

DATA AND RESOURCES

All data used in this paper came from published sources listed in the references.

ACKNOWLEDGMENTS

We thank Profs. Jim Knapp and Tom Owens, and Dr. G. Lin for their suggestions to improve the quality of the manuscript. We are especially appreciative and grateful to Prof. John Ebel for his detailed review. We also thank *SRL* Eastern Section Editor Martin Chapman for his insightful comments. The study was supported by grants from the Savannah River Site and the U.S. Geological Survey.

REFERENCES

Ackermann, H. D. (1983). Seismic-refraction study in the area of the Charleston, South Carolina, 1886 earthquake. In Gohn 1983, F1–F20

Bakun, W. H., and M. G. Hopper (2004). Magnitudes and locations of the 1811–1812 New Madrid, Missouri, and the 1886 Charleston, South Carolina, earthquakes. *Bulletin of the Seismological Society of America* **94**, 64–75.

Bollinger, G. A. (1977). Reinterpretation of the Intensity Data for the 1886 Charleston, South Carolina, earthquake. In *Studies Related to the Charleston, South Carolina, Earthquake of 1886; A Preliminary Report*, ed. D. W. Rankin, 17–32. USGS Professional Paper 1028.

Bollinger, G. A. (1983). Speculations on the nature of seismicity at Charleston, South Carolina, U.S. In Gohn 1983, T1–T11

Burdick, L. J., and G. R. Mellman (1976). Inversion of the body waves from the Borrego Mountain earthquake to the source mechanism. *Bulletin of the Seismological Society of America* **66**, 1,485–1,499.

Burford, R. O. (1968). Continued slip on the Coyote Creek fault after the Borrego Mountain earthquake. In *The Borrego Mountain Earthquake of April 9, 1968*, 105–111. USGS Professional Paper 787.

Colquhoun, D. J., I. D. Woollen, D. S. Van Nieuwenhuise, G. G. Padgett, R. W. Oldham, D. C. Boylan, P. D. Howell, and J. W. Bishop (1983). *Surface and Subsurface Stratigraphy, Structure and Aquifers of the South Carolina Coastal Plain*. Ground Water Protection Division, Report for Department of Health and Environmental Control. Columbia, SC: Office of the Governor, 78 pps.

Dewey, J. (1983). Relocation of instrumentally recorded pre-1974 earthquakes in the South Carolina region. In Gohn 1983, Q1–Q9.

Durá-Gómez, I. (2004). Seismotectonic framework of the Middleton Place Summerville seismic zone near Charleston, South Carolina. MS thesis, University of South Carolina, Columbia, 180 pps.

Dutton, C. E. (1890). *The Charleston Earthquake of August 31, 1886*. USGS Annual Report, Report no. 9, 203–528 (republished in 1975).

Ellsworth, W. L. (1977). Three-dimensional structure of the crust and mantle beneath the island of Hawaii. PhD diss., Massachusetts Institute of Technology, Cambridge, 327 pps.

Garner, J. T. (1998). Re-evaluation of the seismotectonics of the Charleston, South Carolina area. MS thesis, University of South Carolina, Columbia, 250 pps.

Gohn, G. S., ed. (1983). *Studies Related to the Charleston, South Carolina, Earthquake of 1886—Tectonics and Seismicity*. USGS Professional Paper 1313.

Gohn, G. S., B. Houser, and R. R. Schneider (1983). Geology of the lower Mesozoic(?) sedimentary rocks in Clubhouse Crossroads test hole #3, near Charleston, South Carolina. Speculations on the nature of seismicity at Charleston, South Carolina. U.S. In Gohn 1983, D1–D17.

Hamilton, R. M., J. C. Behrendt, and H. D. Ackermann (1983). Land multichannel seismic reflection evidence for tectonic features near Charleston, South Carolina. In Gohn 1983, I1–I18. .

Johnston, A. C. (1996). Seismic moment assessment of earthquakes in stable continental regions, III. New Madrid 1811–1812, Charleston and Lisbon 1755. *Geophysical Journal International* **126**, 314–344.

Lahr, J. C. (1996). *Quick-start Manual for HYPOELLIPSE Version 3.0., A Computer Program for Determining Local Earthquake Hypocentral Parameters, Magnitude, and First-Motion Pattern*. USGS Open-File Report.

Lennon, G. (1985). Identification of a northwest trending seismogenic graben near Charleston. MS thesis, University of South Carolina, Columbia, 84 pps.

Louderback, G. L. (1943). The personal record of Ada M. Trotter of certain aftershocks of the Charleston earthquake of 1886. *Bulletin of the Seismological Society of America* **33**, 199–206.

Madabhushi, S., and P. Talwani (1983). Fault plane solutions and relocations of recent earthquakes in Middleton Place Summerville seismic zone near Charleston, South Carolina. *Bulletin of the Seismological Society of America* **83**, 1,442–1,466.

Marple, R. T. (1994). Discovery of a possible seismogenic fault system beneath the Coastal Plain of South and North Carolina from integration of river morphology and geological and geophysical data. PhD diss., University of South Carolina, Columbia, 354 pps.

McClay, K., and M. Bonora (2001). Analog models of restraining stopovers in strike-slip fault systems. *American Association of Petroleum Geologists Bulletin* **85**, 233–260.

McKinley, C. (1887). A descriptive narrative of the earthquake of August 31, 1886. In *Appendix for the City (of Charleston) Year Book, 1886*, 345–441. Charleston, SC: Walker, Evans, and Cogswell, Co.

Reasenberg, P. A., and D. Oppenheimer (1985). *FPFIT, FPPLOT, and FPPAGE: Fortran Computer Programs for Calculating and Displaying Earthquake Fault-plane Solutions*. USGS Open-File Report 85-0739.

Segall, P., and D. D. Pollard (1980). Mechanics of discontinuous faults. *Journal of Geophysical Research* **85**, 4,337–4,350.

Shedlock, K. M. (1987). *Earthquakes Recorded by the South Carolina Seismic Network*. USGS Open-File Report 87-0437.

Shedlock, K. M. (1988). Seismicity in South Carolina. *Seismological Research Letters* **59**, 165–171.

Sibson, R. H. (1986). Rupture interaction with fault jogs. In *Earthquake Source Mechanics*, ed. S. Das, J. Boatwright, and C. H. Scholz. AGU Geophysical Monograph 37, Maurice Ewing Series 6, 157–167. Washington, DC: American Geophysical Union.

Taber, S. (1914). Seismic activity in the Atlantic Coastal Plain near Charleston, South Carolina. *Bulletin of the Seismological Society of America* **4**, 108–160.

Talwani, P. (1982). Internally consistent pattern of seismicity near Charleston, South Carolina. *Geology* **10**, 654–658.

Talwani, P. (2000). *Velocity Structure Inferred from an Exploratory Oil Well in Colleton County, South Carolina*. Unpublished report, 4 pps.

Talwani, P. (2001). Macroscopic effects of the Charleston earthquake. In *73rd Annual Meeting of the Eastern Section of the Seismological Society of America,* Field Trip Guide, 14 October 2001.

Talwani, P., and I. Durá-Gómez (2009). Finding faults in the Charleston area, South Carolina: 2. Complementary data. *Seismological Research Letters* **80**, 901–919.

Tarr, C., and S. Rhea (1983). Seismicity near Charleston, South Carolina, March 1973 to December 1979. In Gohn 1983, R1–R17.

Tarr, C., P. Talwani, S. Rhea, D. Carver, and D. Amick (1981). Results of recent South Carolina seismological studies. *Bulletin of the Seismological Society of America* **71**, 1,883–1,902.

Waldhauser, F. (2001). *HypoDD: A Program to Compute Double-difference Hypocenter Locations*. USGS Open-File Report 01-113.

Waldhauser, F., and W. L. Ellsworth (2000). A double-difference earthquake location algorithm: Method and application to the northern Hayward fault, California. *Bulletin of the Seismological Society of America* **90**, 1,353–1,368.

Waldhauser, F., and P. G. Richards (2004). Reference events for regional seismic phases at IMS stations in China. *Bulletin of the Seismological Society of America* **94**, 2,265–2,279.

Weems, R. E., and W. C. Lewis (2002). Structural and tectonic setting of the Charleston, South Carolina, region: Evidence from the Tertiary stratigraphy record. *GSA Bulletin* **114**, 24–42.

Zoback, M. D. (1983). Intraplate earthquakes, crustal deformation, and in-situ stress. In *A Workshop on the 1886 Charleston, South Carolina, Earthquake and Its Implications for Today*, ed. W. W. Hays and P. L. Gori, 169–178. USGS Open-File Report 83-843.

Department of Geological Sciences
University of South Carolina
701 Sumter Street
Columbia, South Carolina 29208 U.S.A.
idura@geol.sc.edu
(I.D.-G.)